Colloids and Surfaces A 595 (2020) 124679

Contents lists available at ScienceDirect

Colloids and Surfaces A

journal homepage: www.elsevier.com/locate/colsurfa

Synthesis of citrate–modified $CuFeS_2$ catalyst with significant effect on the photo–Fenton degradation efficiency of bisphenol a under visible light and near–neutral pH

Julia da Silveira Salla[a], Katia da Boit Martinello[b,*], Guilherme L. Dotto[a,**], Esmeralda García-Díaz[c], Hassan Javed[d], Pedro J.J. Alvarez[d], Edson Luiz Foletto[a]

[a] Graduate Program in Chemical Engineering, Universidade Federal de Santa Maria, 97105–900, Santa Maria, Brazil
[b] Departamento de Civil y Ambiental, Universidad de La Costa, Calle 58 #55-66, CP, 080002, Barranquilla, Atlántico, Colombia
[c] Chemistry Center, Universidad Autónoma de Puebla, 72570, Puebla, Mexico
[d] Department of Civil and Environmental Engineering, Rice University, 77005, Houston, United States

GRAPHICAL ABSTRACT

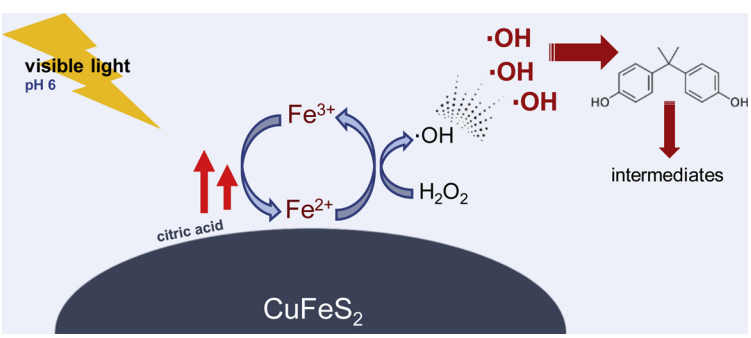

ARTICLE INFO

Keywords:
$CuFeS_2$
Citric acid
Photo–Fenton
Bisphenol A
Intermediates
Hydroxyl radical

ABSTRACT

In this study, for the first time, citric acid was employed as a chelating agent in $CuFeS_2$ synthesis in order to accelerate the regeneration of Fe^{2+} during the photo–Fenton reaction, promoting a faster production of ˙OH radicals. The novel $CuFeS_2$ material showed remarkable catalytic efficiency for bisphenol A (BPA) degradation during the photo–Fenton process under visible light and near–natural pH, with a rate 10 times faster than that of $CuFeS_2$ prepared without citrate. Furthermore, $CuFeS_2$ promoted rapid generation of ˙OH radicals and showed efficient H_2O_2 consumption, sustaining the catalytic efficiency and stability even after 4 consecutive cycles of use. $CuFeS_2$ was also efficient for BPA degradation from a municipal wastewater treatment plant effluent. BPA by–products were identified and a mechanism for BPA degradation was proposed. After the photo–Fenton process, no Fe^{3+} species were identified on the catalyst surface by X–ray photoelectron spectroscopy (XPS), indicating that citric acid accelerated the conversion of Fe^{3+}/Fe^{2+}, thus increasing the generation of ˙OH and the process efficiency.

* Corresponding author.
** Corresponding author at: Chemical Engineering Department, Federal University of Santa Maria, UFSM, 1000, Roraima Avenue, 97105–900, Santa Maria, RS, Brazil.
E-mail addresses: katiamartinello@yahoo.com.br (K. da Boit Martinello), guilherme.dotto@ufsm.br (G.L. Dotto).

https://doi.org/10.1016/j.colsurfa.2020.124679
Received 12 January 2020; Received in revised form 7 March 2020; Accepted 9 March 2020
Available online 10 March 2020
0927-7757/ © 2020 Elsevier B.V. All rights reserved.

1. Introduction

Advanced oxidation processes (AOPs) are receiving increasing interest to eliminate relatively recalcitrant water contaminants of emerging concern, such as bisphenol A [1,2]. AOPs are centered on the generation of reactive oxygen species (ROS), such as hydroxyl radical ($^{\cdot}OH$) and superoxide anion radical ($O_2^{\cdot}$–), capable of degrading several types of organic contaminants [3,4]. In the Fenton process, ROS are initially generated from the catalytic decomposition of H_2O_2 by Fe^{2+} (Eq. 1), and the oxidized Fe^{3+} species can be reduced by H_2O_2 to regenerate Fe^{2+} (Eq. 2) [5,6].

$$Fe^{2+} + H_2O_2 \rightarrow Fe^{3+} + {}^{\cdot}OH + OH\text{–}k_1 = 40\text{–}80\ M^{-1}\ s^{-1} \quad (1)$$

$$Fe^{3+} + H_2O_2 \rightarrow Fe^{2+} + HO_2^{\cdot} + H^+ k_2 = 0.001 - 0.01\ M^{-1}\ s^{-1} \quad (2)$$

Compared to the homogeneous Fenton process, which has catalytic efficacy only at strictly acidic pH (≈ 3.0) and produces high amounts of iron sludge, the heterogeneous process stabilizes iron on the catalyst surface and decomposes H_2O_2 over a greater pH range without precipitation of iron hydroxide. In addition, the catalyst can be easily recovered and reused in the system [5,6].

The rate–limiting step of the heterogeneous Fenton process is the regeneration of Fe^{2+} (Eq. 2), due to the low rate constant, which is an important determinant of the overall treatment efficiency [6,7]. To overcome this drawback, many studies have dedicated on introducing chelating agents to the Fenton process, such as citric acid, oxalic acid, hydroxylamine and EDTA [8–10]. Chelating agents can form complexes with metal ions and drastically affect their redox properties. The addition of citric acid changes the redox potential of Fe^{3+}/Fe^{2+} from 0.77 eV to 0.37 eV (pH 7 and 25 °C) [8]. The reduced Fe^{2+} can be reoxidized by H_2O_2, enhancing the production of ROS by the decomposition of H_2O_2, and the process efficiency could be improved.

Chalcopyrite ($CuFeS_2$) is a semiconductor that belongs to the family of chalcogenides. It has a mixed valence of copper and iron that opens a potential for highly effective electron transfer on its surface [11]. Despite being well known for its conductivity and for having unusual electrical and magnetic proprieties, the use of $CuFeS_2$ as a catalyst for AOPs is poorly explored [12,13]. Moreover, $CuFeS_2$ is a visible–light activated photocatalyst with low band gap energy (< 1 eV) [12,14] and its copper atoms can (similarly to iron) also decompose H_2O_2 into ROS [15].

In this study, for the first time, $CuFeS_2$ was synthesized with the addition of citric acid as a chelating agent and used as a heterogeneous catalyst in the photo–Fenton reaction to remove bisphenol A (BPA) from an aqueous solution and a municipal wastewater treatment plant effluent. The catalyst surface was analyzed by XPS, before and after its use in the process, to verify changes in the Fe^{3+}/Fe^{2+} redox potential. Moreover, the stability and reuse of the catalyst were evaluated, as well as the ROS and H_2O_2 residual concentration, during the photo–Fenton process under visible light and near–neutral pH. The BPA degradation by–products were identified and a mechanism for the process was proposed.

2. Materials and methods

2.1. Synthesis of $CuFeS_2$

The synthesis of $CuFeS_2$ powder was performed by the microwave–assisted method. The preparation started with the addition of 3 mmol of copper chloride (CuCl; Sigma–Aldrich), 3 mmol of iron (III) chloride hexahydrate ($FeCl_3{\cdot}6H_2O$; Sigma–Aldrich), 6 mmol of citric acid ($C_6H_8O_7$; Sigma–Aldrich) and 7.5 mmol of thiourea ($(NH_2)_2CS$; Sigma–Aldrich) in 40 mL of distilled water under constant stirring to obtain a homogeneous solution. After 30 min, the solution was transferred to a microwave oven (Milestone, Ethos One, Germany) operating at 200 °C and 1400 W for 7 min. The precipitates formed were filtered, washed 3 times with distilled water and dried under vacuum at room temperature.

2.2. Characterization

X-ray powder diffraction (XRD) spectroscopy was employed to identify the phases of $CuFeS_2$ samples in a Miniflex 300 diffractometer (Rigaku), with Cu-Kα radiation under operational conditions of 30 kV and 10 mA. N_2 adsorption-desorption isotherms were performed on an ASAP 2020 instrument. The morphology were recorded by scanning electron microscopy (SEM; Sigma 300 V P) and transmission electron microscopy (TEM; JEOL-JEM-1011). The surface was characterized by X–ray photoelectron spectroscopy (XPS) in a VSW HA–100 spherical analyzer, before and after $CuFeS_2$ was used as a catalyst in the photo–Fenton process. MgKα radiation was applied (1253.6 eV) and the binding energy calibration was based on C1s at 284.6 eV. The zeta potential of $CuFeS_2$ was determined by phase analysis light scattering with a Zen 3600 Zetasizer (Malvern Instruments) to evaluate the surface charge.

2.3. Catalytic tests

For the photo–Fenton catalytic tests, 6 fluorescent lamps (4 W, F4T5/HLK) were installed around the reactor, providing a total light intensity of 18 W m^{-2}. After determining the ideal operating conditions to maximize the BPA degradation (Fig. S1), the photo–Fenton catalytic tests were performed as follows: 50 mL of BPA solution (20 mg L^{-1}; pH 6.0) were placed in a beaker under constant stirring and temperature (25 °C). The catalyst (0.2 g L^{-1} of $CuFeS_2$) was dispersed in the solution, and the system was kept in the dark for 30 min to reach adsorption equilibrium. Then, 20 mmol L^{-1} of H_2O_2 (30 %) were added to the system and, immediately, the visible light irradiation was turned on. Aliquots were taken at predetermined intervals, the catalyst was filtered out using a 0.22 μm PTFE syringe filter and the solution was analyzed for determination of BPA degradation.

After each assay, the solid and liquid phases were separated by simple precipitation. The liquid was used for Fe and Cu leaching analysis. The solid was washed 3 times with distilled water and filtered using a 0.22 μm PTFE syringe filter to be used again in reuse tests.

Experiments were also performed to evaluate the catalytic capacity of $CuFeS_2$, using a municipal effluent from a tertiary wastewater treatment plant (WWTP), and to investigate the potential interference of background organic matter. BPA (20 mg L^{-1}) was mixed with the effluent from the West University Place WWTP in Houston (Texas, USA) and subjected to concurrent adsorption and photo–Fenton degradation with $CuFeS_2$ as described above. The characteristics of the WWTP effluent have been reported elsewhere [16].

In order to determine which major oxidants are responsible for BPA degradation during the $CuFeS_2$–catalyzed photo–Fenton reaction, tests were conducted in the presence of different ROS scavengers. The scavengers tested included 1 mmol L^{-1} of *t*–butanol for $^{\cdot}OH$ and 1 mmol L^{-1} of *p*–benzoquinone for $O_2^{\cdot}$– [17].

Coumarin was used as a probe to measure, indirectly, the production of $^{\cdot}OH$ radicals during the photo–Fenton reaction [18,19]. Coumarin reacts with the $^{\cdot}OH$ radicals and produces 7–hydroxycoumarin, according to Scheme 1.

It was used 50 mL of coumarin (0.1 mmol L^{-1} and pH 6.0) instead of BPA solution, and a similar procedure as described above was followed. Aliquots were analyzed for 7–hydroxycoumarin fluorescence intensity. A calibration curve using 7–hydroxycoumarin as a standard was constructed to quantify the product formed. The steady–state concentration of hydroxyl radicals was determined based on the comparation between the yields of 7–hydroxycoumarin and $^{\cdot}OH$ generation. It was reported that 6.1 % of $^{\cdot}OH$ can be detected as 7–hydroxycoumarin [18,20].

The determination of residual H_2O_2 concentration was performed indirectly by the metavanadate method [21]. In a volumetric flask was

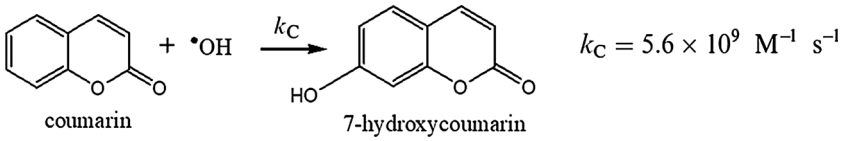

Scheme 1. Reaction between coumarin and ˙OH to generate 7–hydroxycoumarin.

added 1 mL of ammonium metavanadate (6.2 mmol L^{-1}), 8 mL of sulfuric acid (0.058 mol L^{-1}) and 1 mL of sample from the photo–Fenton catalytic test. The reaction between H_2O_2 and ammonium metavanadate produces peroxivanadium cation (VO_2^{3+}), wich has orange–red color. A calibration curve was prepared to relate the H_2O_2 and the VO_2^{3+} concentrations.

2.4. Analytical methods

The concentration of BPA was analyzed using high–performance liquid chromatography (HPLC; LC–20AT; Shimadzu) equipped with a UV–vis detector (SPD–M20A; Shimadzu) and a Shimadzu C18 5 µm 50 × 4.6 mm column. The mobile phase was acetonitrile (40 %) and water (60 %), with a flow rate of 1 mL min^{-1} and an injection volume of 40 µL. The wavelength analyzed was 218 nm, which was determined using the UV–vis absorption spectrum of BPA.

The by–products were identified using liquid chromatography–mass spectrometry (LC–MS; MicroToF–ESI; Bruker) equipped with a 1200 HPLC (Agilent) and a Scherzo SM–C18 3 µm 50 × 2 mm (Imtakt) column. The mobile phase was 0.1 % formic acid in water (98 %) and 0.1 % formic acid in acetonitrile (2%), with a flow rate of 0.3 mL min^{-1} and an injection volume of 10 µL.

The total organic carbon was determined by a TOC analyzer (TOC–V_{CSH}; Shimadzu). The concentration of leached Fe and Cu was determined by inductively coupled plasma optical emission spectrometer (ICP–OES; Optima 8300; Perkin Elmer).

7–hydroxycoumarin fluorescence intensity was analyzed in a FL–1000 spectrometer (HORIBA), with an excitation wavelength of 340 nm and a range from 380 to 640 nm as the emission wavelength. Peroxivanadium cation (VO_2^{3+}) was measured at 450 nm by a UV–vis spectrophotometer (Ultrospec 2100 *pro*; Amersham Biosciences).

3. Results and discussion

3.1. BPA degradation by $CuFeS_2$–catalyzed photo–Fenton process

Comparative assays were performed to verify the photo–Fenton catalytic activity of $CuFeS_2$ for BPA degradation. Tests to evaluate the BPA adsorption using $CuFeS_2$ were performed in the dark, and only 5% was adsorbed on the catalyst surface within 30 min. Moreover, BPA degradation in the presence of H_2O_2 and visible light irradiation may be negligible, as only 8% of BPA was degraded within 60 min of reaction. Apparently, H_2O_2 weakly absorbs visible light and, therefore, has low oxidation capacity [22].

Tests that showed important catalytic efficiency are shown in Fig. 1. BPA degradation by the photo–Fenton process was evaluated using $CuFeS_2$ prepared with and without the addition of citric acid during the synthesis process. From the results presented in Fig. 1(a), it is explicit that $CuFeS_2$ prepared with citric acid promoted a faster and more efficient degradation of BPA, prominent mainly in the first 15 min of the photo–Fenton reaction, when 90 % of degradation was observed. These results further indicated that the addition of citric acid during the synthesis of $CuFeS_2$ caused a significant increase in the catalytic activity of the material.

The degradation kinetic of BPA by the $CuFeS_2$–catalyzed photo–Fenton process is consistent with the pseudo–first order kinetic model, according to Fig. 1(b). The observed kinetic constants were determined from the regression curves of –ln C/C_0 *versus* irradiation time. The kinetic constant for $CuFeS_2$ synthetized with citric acid

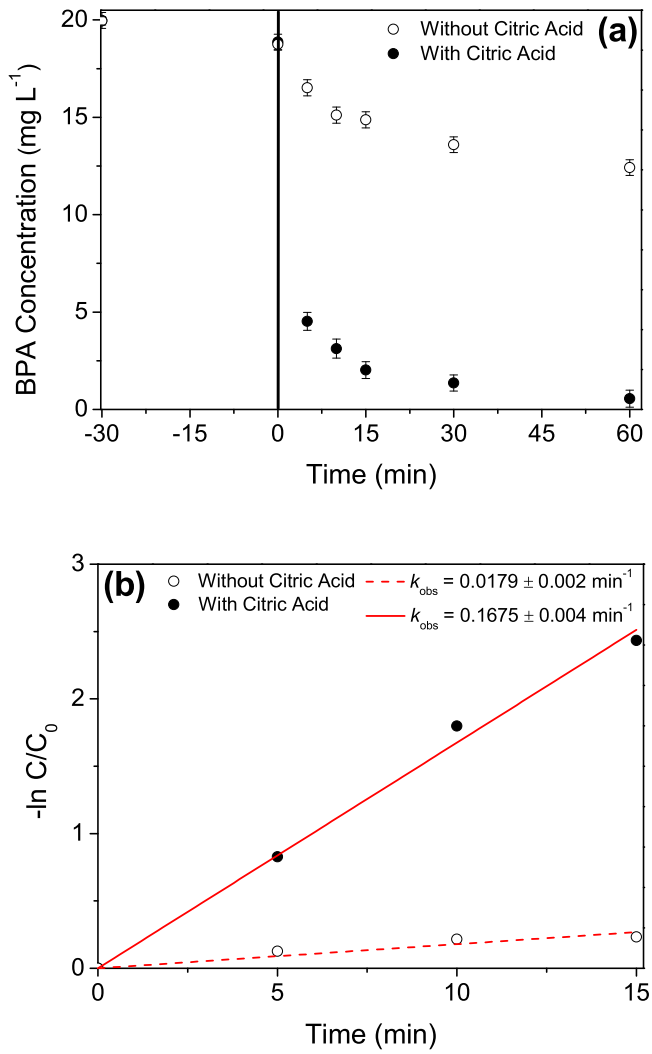

Fig. 1. (a) Kinetics of BPA degradation by the $CuFeS_2$–catalyzed photo–Fenton process and (b) Pseudo–first order fitting for the kinetic data (pH = 6.0; [BPA] = 20 mg L^{-1}; [H_2O_2] = 20 mmol L^{-1}; [$CuFeS_2$] = 0.2 g L^{-1}).

(k_{obs} = 0.1675 ± 0.004 min^{-1}; R^2 = 0.9971) was about 10 times higher than that for $CuFeS_2$ synthetized without citric acid (k_{obs} = 0.0179 ± 0.002 min^{-1}; R^2 = 0.9532). Thus, $CuFeS_2$ with citric acid had superior catalytic performance in the photo–Fenton degradation of BPA, reaching 97 % of degradation.

The oxidation of organic compounds by the photo-Fenton process occurs through two initial steps, represented by Eq. 1 and 2. The rate-limiting step is shown in Eq. 2, due to the accumulation of Fe(III) and the poor regeneration of Fe(II) [9]. Meanwhile, the reaction of Fe(III) and H_2O_2 generates $O_2^{\cdot}$–, whose oxidation ability is much less than ˙OH [10]. The results from Fig. 1 suggest that the presence of citric acid in $CuFeS_2$ compound effectively avoided the Fe(III) accumulation and accelerated the Fe(III)/Fe(II) redox cycles, when compared to $CuFeS_2$ without citric acid, leading to a greater efficiency and increased the pseudo first-order reaction rate.

Given these encouraging results with $CuFeS_2$ prepared with citric acid, only this compound will be further studied in this work as a

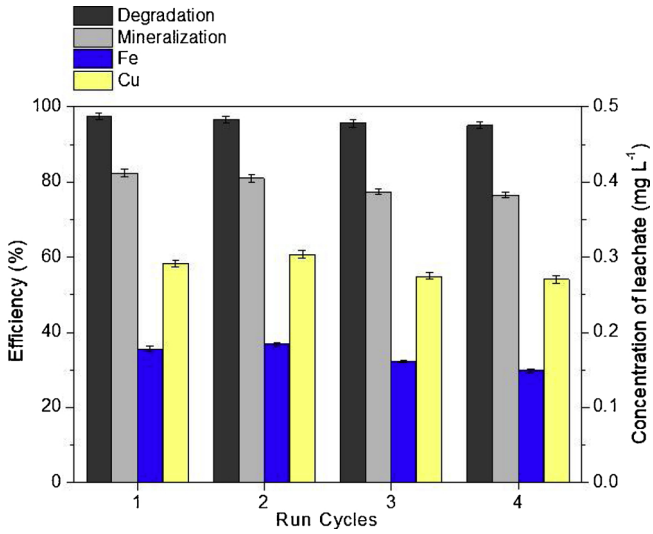

Fig. 2. $CuFeS_2$ stability and reusability over 4 cycles of use.

catalyst in the photo–Fenton process for BPA degradation.

3.2. $CuFeS_2$ stability and reusability

The stability and reusability of $CuFeS_2$ catalyst were investigated during 4 consecutive cycles of use in the photo–Fenton process, according to Fig. 2.

The photo–Fenton catalytic activity of $CuFeS_2$ for BPA degradation (97.4 %) and TOC mineralization (82.3 %), during the first use of the material, remained balanced during all the cycles analyzed. After the fourth use, the degradation efficiency reached 95.1 % and the TOC mineralization efficiency was 76.6 % after 60 min of reaction. In addition, a maximum concentration of 0.18 mg L^{-1} of Fe and 0.30 mg L^{-1} of Cu leached into the solution. This concentration represents less than 0.5 % of the total amount of Fe and Cu presented in the catalyst at the beginning of the reaction. The results reveal that the catalyst has a great stability and a potential application value for, at least, 4 cycles of use.

3.3. Active free radicals and H_2O_2 residual concentration

To further elucidate the effect of $CuFeS_2$ as a catalyst, a study of the potential free radicals present in the system was performed, as well as the decomposition of H_2O_2 during the reaction (Fig. 3).

Fig. 3(a) indicated that the addition of *t*–butanol had a negative influence on the BPA degradation efficiency, completely decreasing the rate constant, implying that the scavenger consumed the $^{\cdot}OH$ radicals present in solution. In contrast, the addition of *p*–benzoquinone, an $^{\cdot}O_2$– scavenger, did not inhibit the BPA degradation, implying that the radical was not present in the system during the reaction. The results suggest that the $^{\cdot}OH$ radicals were the species responsible for BPA degradation during the $CuFeS_2$–catalyzed photo–Fenton reaction, which agrees well with previous results [23].

The generation of 7–hydroxycoumarin under visible light was shown in Fig. 3(b). The highest fluorescence intensity of 7–hydroxycoumarin, at 530 nm, was observed in the first 5 min of the photo–-Fenton reaction, further confirming the presence of $^{\cdot}OH$ radicals.

The concentration of $^{\cdot}OH$ radicals increased rapidly at the beginning of the reaction, as shown in Fig. 3(c), and presented its maximum concentration of 0.09 mmol L^{-1} in 5 min. At this stage, the highest $^{\cdot}OH$ production rate was due to the decomposition of H_2O_2 by $CuFeS_2$. After that, the $^{\cdot}OH$ concentration started to decrease while the radicals were consumed for BPA degradation. The radicals were completely consumed at the end of the photo–Fenton reaction when about 100 % of BPA has been degraded.

The decomposition of H_2O_2 during the BPA degradation by the $CuFeS_2$–catalyzed photo–Fenton process was shown in Fig. 3(d). Within 15 min, where the highest degradation efficiency of BPA was observed, about 86 % of the H_2O_2 initially added was consumed and, after 60 min, 95 % of the H_2O_2 was decomposed by $CuFeS_2$.

3.4. $CuFeS_2$ characterization

The XRD patterns of $CuFeS_2$ samples are presented in Fig. 4(a) and (b), respectively. The XRD result is the only one presented for $CuFeS_2$ modified or not by citric acid, since it was the studied analysis that showed a significant difference between the two materials.

The results showed that both procedures can form $CuFeS_2$ phase, corresponding to the crystallographic plan reported by JCPDS 37-0471. The diffraction peaks at $2\theta = 29.37°$, 48.65° and 57.85° correspond to the (112), (220)/(204) and (312)/(116) lattice planes [24,25]. However, other unwanted phases such as CuS and Fe_2O_3 were also formed when citric acid was not added to the material preparation. With the addition of citric acid as a chelating agent, it was expected that the random reaction of Cu or Fe cation with S could be prevented, and the reaction of the two chelated cations by citric acid would proceed simultaneously with S. Thus, the unwanted phases in the $CuFeS_2$ compound could be avoided. This result was also observed in other studies [24].

SEM and TEM images of $CuFeS_2$ are presented in Fig. 4(c) and (d), respectively. The morphology exhibited particles with a rough and irregular surface in nanometric scale. Furthermore, $CuFeS_2$ had spherical morphology and porous surface, which has been reported in other studies [25].

From the N_2 adsorption-desorption analysis presented in Fig. S2, properties such as surface area and total pore volume were obtained. For $CuFeS_2$, the BET surface area was 3.94 m^2 g^{-1} and the BJH total pore volume was 0.017 cm^3 g^{-1}.

Since ROS are known to be unstable, short lived and highly reactive, they can be decomposed or scavenged rapidly before reaching the pollutant molecules. Therefore, the proximity between these compounds and the catalyst surface is important in AOPs [26]. Zeta potential of $CuFeS_2$ was measured at pH 6.0 and its surface was negatively charged under this condition. On the other hand, BPA is slightly alkaline with a pKa value of 9.6 [27] and predominates in the acidic form (positively charged) at pH 6.0. The existence of compatibility charges between $CuFeS_2$ and BPA at pH 6.0 favors the electrostatic attraction between the contaminant and the catalyst surface, where the $^{\cdot}OH$ radicals could be present.

The chemical state of iron on $CuFeS_2$ surface was examined by XPS analysis. The respective results are shown in Fig. 5.

Fig. 5(a) and (b) displays the XPS spectra in the Fe2p region for $CuFeS_2$, before and after the photo–Fenton process, respectively. For the fresh sample, the peaks corresponding to Fe^{2+} are located at 707.3, 709.1, 720.3 and 722.2 eV, and the peaks corresponding to Fe^{3+} are located at 711.3 and 717.9 eV [28–30]. For both samples, the peak around 707 eV can be assigned to the binding energy of Fe^{2+} bonded to sulfur [30]. In addition, the peaks at 709.2 and 720.3 eV in Fig. 5(b) are also attributed to Fe^{2+}. After the process, peaks related to Fe in the +3 oxidation state were not observed. It indicates that the reduction of Fe^{3+} to Fe^{2+} on the $CuFeS_2$ surface was accelerated by the strategy of modifying catalyst synthesis with the addition of citric acid (chelating agent). The redox cycling of Fe^{3+}/Fe^{2+} could be achieved in the photo–Fenton reaction and imply an increase of the BPA degradation rate. Moreover, the peak at 712.7 eV does not match with known peaks of iron species and is assigned to a Cu Auger peak as a consequence of X–ray excitation [30].

The chemical state of copper and sulfur on $CuFeS_2$ surface, before and after its use as a catalyst in the photo–Fenton process, were also examined by XPS analysis. Furthermore, the presence of peaks in the C1s spectrum indicated that citric acid was bound to $CuFeS_2$ surface.

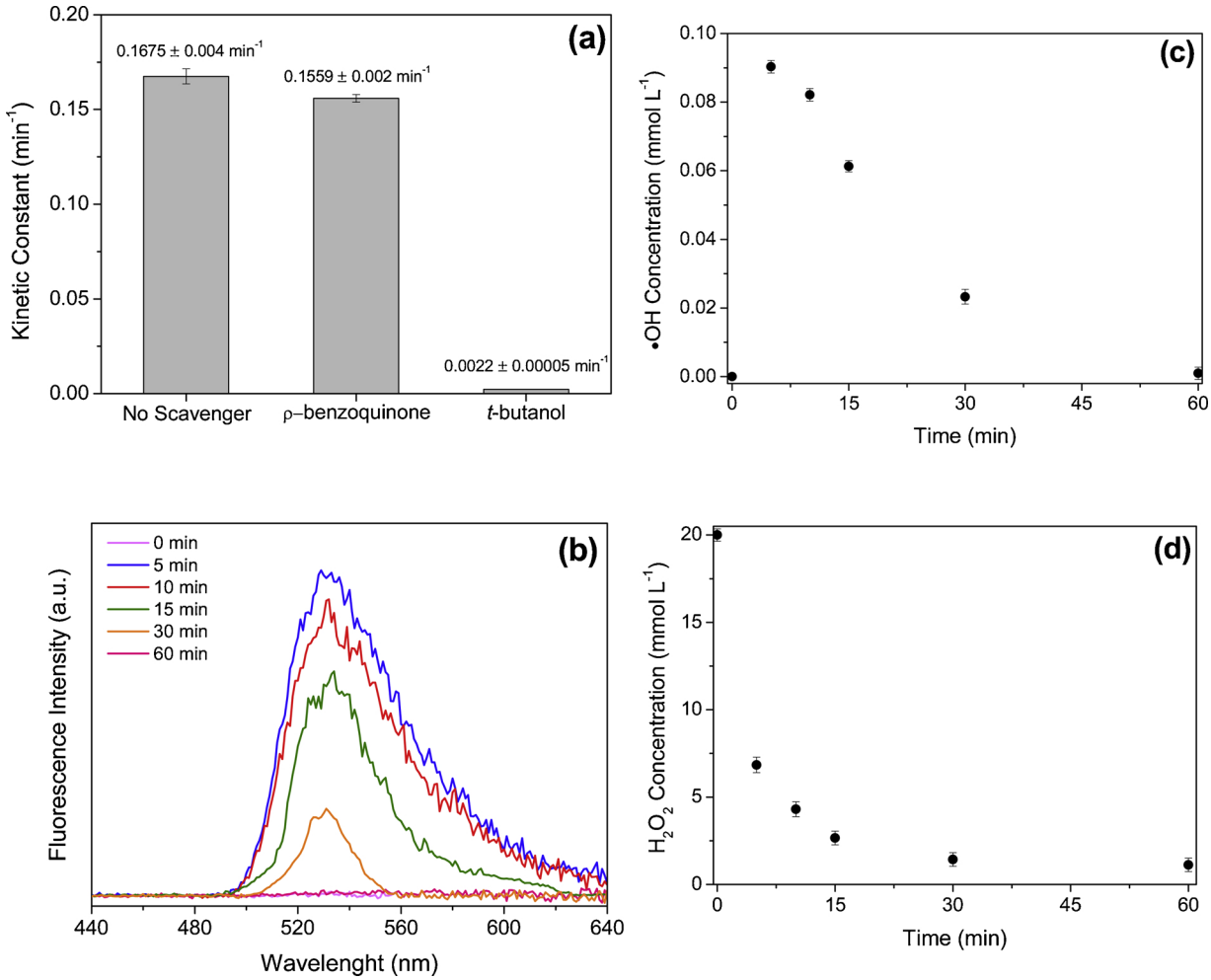

Fig. 3. (a) Pseudo–first order kinetic constant of BPA degradation in the presence of ROS scavengers; (b) 7–hydroxycoumarin fluorescence intensity; (c) Concentration of ˙OH radicals and (d) Decomposition of H_2O_2 during the photo–Fenton process.

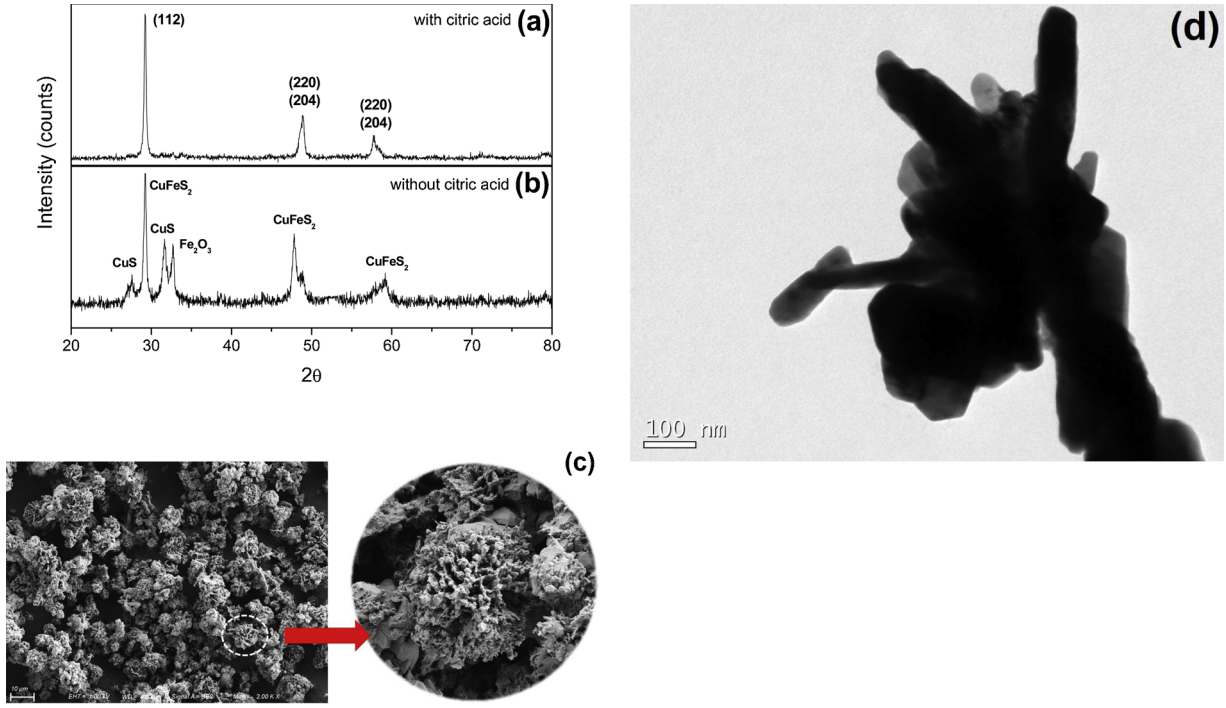

Fig. 4. XRD patterns of $CuFeS_2$ prepared (a) with and (b) without citric acid; (c) SEM and (d) TEM images of $CuFeS_2$ prepared with citric acid.

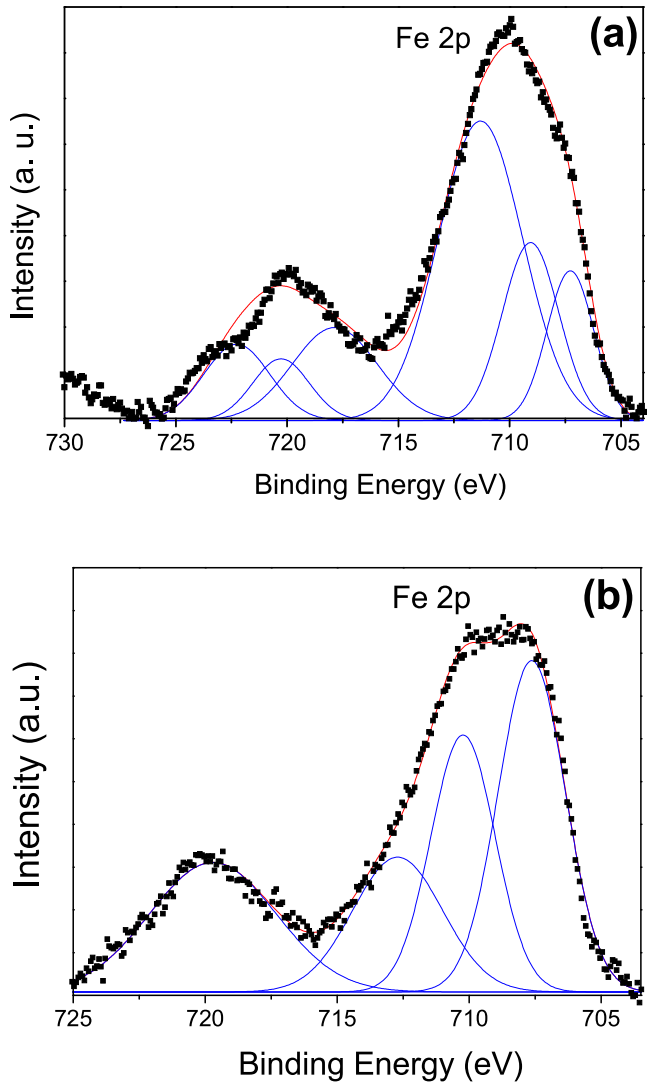

Fig. 5. XPS spectra Fe2p for $CuFeS_2$ before (a) and after (b) the photo–Fenton process.

The spectra and their discussions can be found in Fig. S3.

3.5. By–products and proposed degradation mechanism

Along with the BPA decomposition by the action of hydroxyl radicals, the emergence of several intermediates can be observed until possible mineralization in CO_2 and H_2O [31]. To further elucidate the by–products produced from the BPA degradation by $CuFeS_2$–catalyzed photo–Fenton process, the total ion chromatogram (TIC) is provided in Fig. 6.

For the initial BPA concentration (20 mg L^{-1}) in Fig. 6(a), the peak identified at 19.9 min is characteristic of the bisphenol A compound (m/z 227). According to Fig. 6(b), at least four new peaks of considerable intensity were identified as by–products from the BPA degradation. Table 1 presents the listed peaks in Fig. 6, as well as the retention time (t_R), chemical formula, name and exact mass of the molecular ion (m/z) of each one.

A possible decomposition pathway for BPA was proposed in Scheme 2. Initially, the ˙OH radicals attack the benzene ring of the BPA molecule to form hydroxylated derivates [32,33]. The instability of this intermediate is subjected to cleavage, causing the break into smaller molecules, generating by–products such as 4–isopropylphenol, 4–hydroxyacetophenone, 2–methoxyhydroquinone and 4–(1–hydroxy–1–methylethyl)benzene–1,2–diol [34–36]. In subsequent steps, the intermediates are likely to undergo ring opening reactions to form typical BPA degradation by–products, such as fumaric acid, oxalic acid and isobutyric acid. Finally, by the action of ˙OH, the by–products can be decomposed until their complete mineralization in the final products, CO_2 and H_2O.

In particular, intermediates with m/z close or below 100 can hardly be detected by LC–MS due to limitations of the analysis [32].

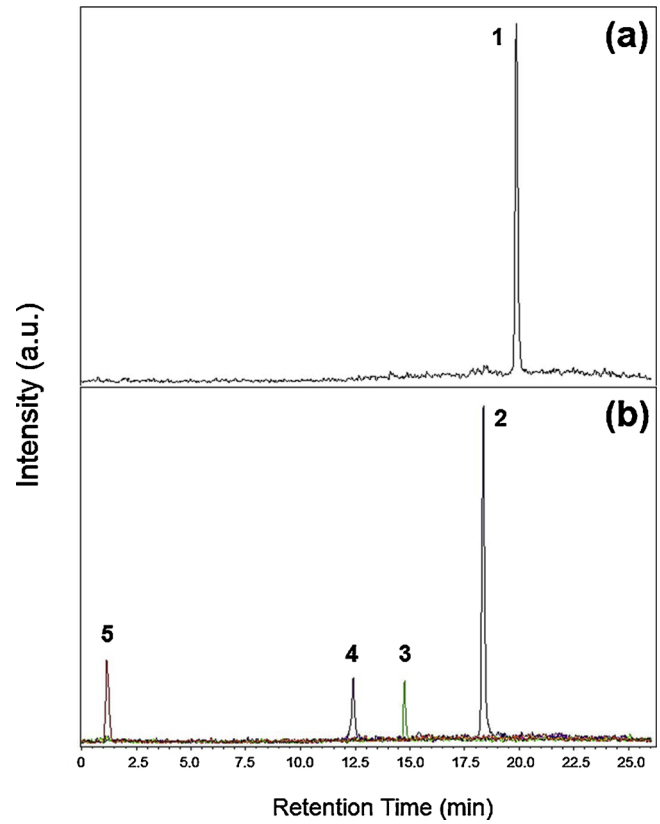

Fig. 6. TIC obtained from the LC–MS analysis of (a) BPA solution (20 mg L^{-1}) and (b) BPA degradation by $CuFeS_2$–catalyzed photo–Fenton reaction.

Table 1
Possible by–products identified from the $CuFeS_2$–catalyzed photo–Fenton reaction for BPA degradation.

Peak	t_R (min)	Formula	Name	m/z
1	19.9	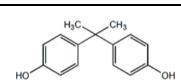	bisphenol A	227
2	18.4	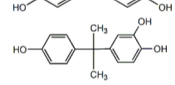	hydroxylated bisphenol A derivates	243
3	14.8	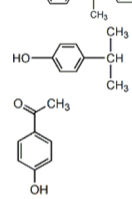	4-isopropylphenol 4-hydroxyacetophenone	135
4	12.4	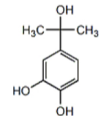	4-(1-hydroxy-1-methylethyl) benzene-1,2-diol	167
5	1.2	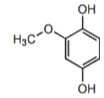	2-methoxyhydroquinone	139

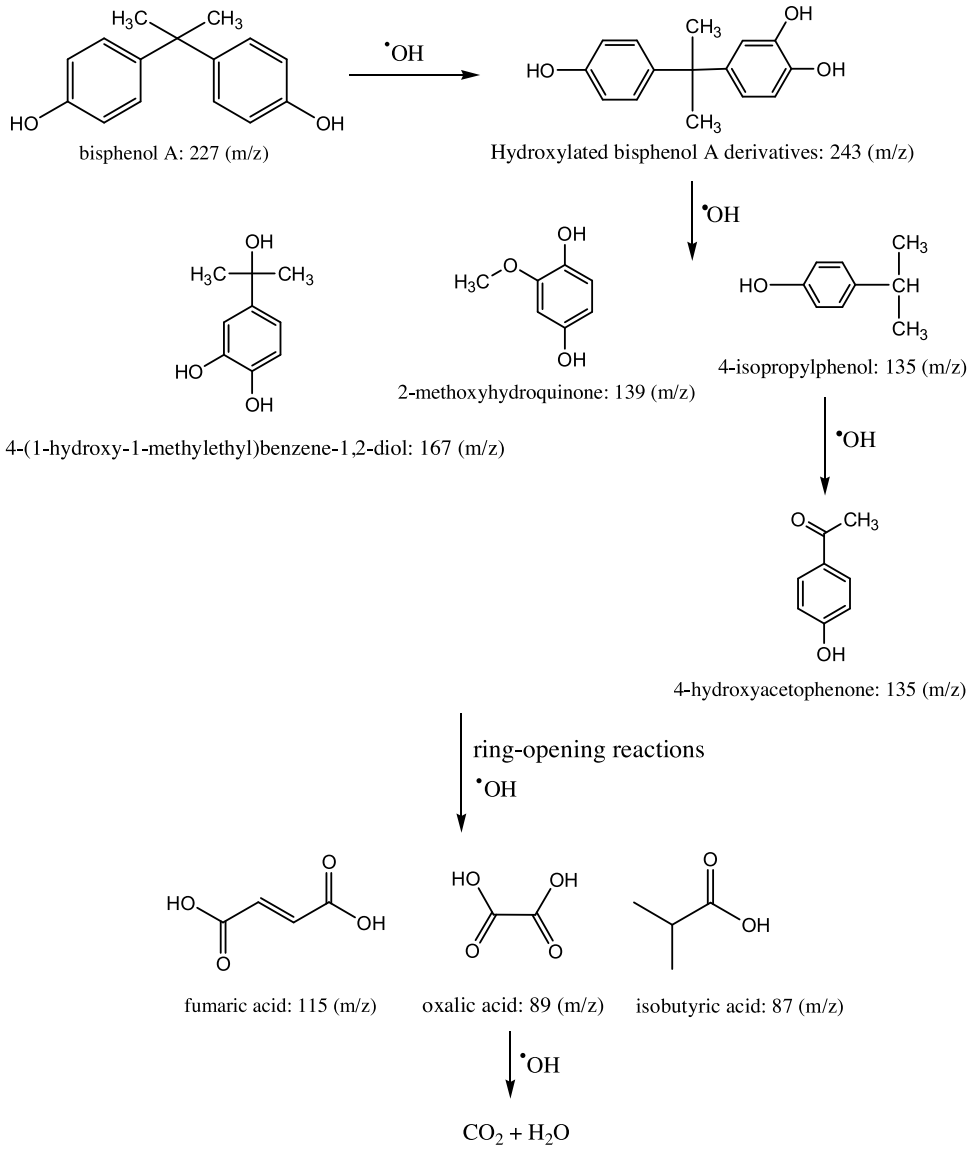

Scheme 2. Possible pathway for BPA degradation induced by $CuFeS_2$–catalyzed photo–Fenton reaction.

The chromatograms for BPA degradation during the $CuFeS_2$–catalyzed photo–Fenton reaction are shown in Fig. 7.

According to Fig. 7(a), from the removal of BPA in deionized water, it was clearly noted that all the peaks that emerged during the photo–Fenton reaction were further transformed and degraded in 60 min. At the end of the process, 97.4 % of BPA has been removed from the system. However, in Fig. 7(b), the presence of background organic matter impaired the process, reducing the efficiency by 24 % and reaching a maximum of 73.4 % of BPA degradation within 60 min. The degradation efficiency was affected due to the presence of other compounds in the real effluent, such as carbonates/bicarbonates, nitrates/nitrites, sulphates, phosphates, chlorides and turbidity, and the non–-selectivity of the ˙OH radicals [37].

4. Conclusions

The use of citric acid during $CuFeS_2$ synthesis changed the Fe^{3+}/Fe^{2+} redox potential during the photo–Fenton process, which facilitated the regeneration of Fe^{2+} species and promoted an increase in the generation of ˙OH radicals. The ˙OH radicals readily reached the BPA molecule due to the proximity between the contaminant and the catalyst surface, resulting of the compatibility of surface charges, and a significant degradation efficiency was observed in both water and wastewater systems. Moreover, along with the fact that $CuFeS_2$ is an easily prepared material, its use as a catalyst in the photo–Fenton process under visible light and near neutral pH showed a powerful generation of ˙OH radicals and achieved a complete degradation of BPA. In summary, the results indicate that the citrate–modified $CuFeS_2$ material is a promising catalyst for the photo–Fenton process, and further improvements on selectivity for ˙OH radicals would make this approach appealing for practical applications in wastewater treatment.

CRediT authorship contribution statement

Julia da Silveira Salla: Conceptualization, Investigation, Resources, Writing - original draft. **Katia da Boit Martinello:** Conceptualization, Methodology, Writing - original draft. **Guilherme L. Dotto:** Conceptualization, Methodology, Funding acquisition. **Esmeralda García-Díaz:** Conceptualization, Writing - review & editing. **Hassan Javed:** Conceptualization, Writing - review & editing. **Pedro J.J. Alvarez:** Conceptualization, Writing - review & editing. **Edson Luiz Foletto:** Conceptualization, Methodology, Formal analysis, Writing - original draft, Visualization.

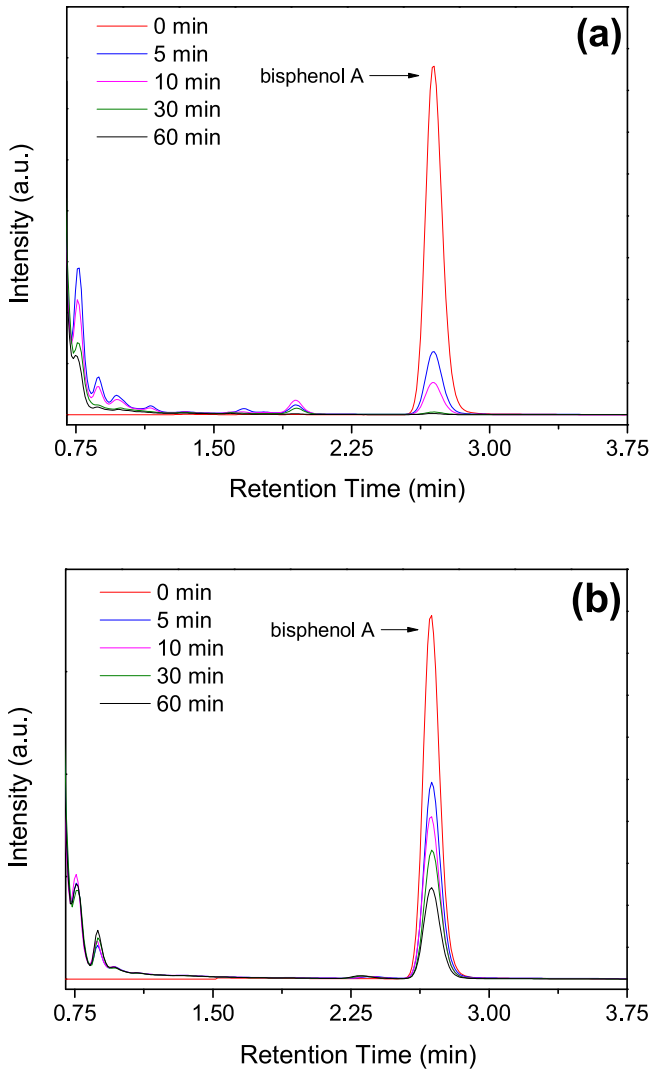

Fig. 7. HPLC chromatogram of BPA degradation in: (a) deionized water and (b) municipal effluent from WWTP.

Declaration of Competing Interest

The authors declare that they have no known competing financial interests or personal relationships that could have appeared to influence the work reported in this paper.

Acknowledgments

This study was financed in part by the Coordenação de Aperfeiçoamento de Pessoal de Nível Superior – Brasil (CAPES) – Finance Code 001 – Process nº 88881.187674/2018–01 – PDSE, and by the Conselho Nacional de Desenvolvimento Científico e Tecnológico – Brasil (CNPq).

Appendix A. Supplementary data

Supplementary material related to this article can be found, in the online version, at doi:https://doi.org/10.1016/j.colsurfa.2020.124679.

References

[1] S. Chakma, V.S. Moholkar, Investigations in synergism of hybrid advanced oxidation processes with combinations of sonolysis + Fenton process + UV for degradation of bisphenol A, Ind. Eng. Chem. Res. 53 (2014) 6855–6865, https://doi.org/10.1021/ie500474f.

[2] D. Zhang, C. Lee, H. Javed, P. Yu, J.–H. Kim, P.J.J. Alvarez, Easily recoverable, micrometer–sized TiO_2 hierarchical spheres decorated with cyclodextrin for enhanced photocatalytic degradation of organic micropollutants, Environ. Sci. Technol. 52 (2018) 12402–12411, https://doi.org/10.1021/acs.est.8b04301.

[3] P. Grassi, F.C. Drumm, J. Georgin, D.S.P. Franco, E.L. Foletto, G.L. Dotto, S.L. Jahn, Water treatment plant sludge as iron source to catalyze a heterogeneous photo–Fenton reaction, Environ. Technol. Inno 17 (2020) 100544, , https://doi.org/10.1016/j.eti.2019.100544.

[4] J. Madhavan, P.S.S. Kumar, S. Anandan, F. Grieser, M. Ashokkumar, Sonophotocatalytic degradation of monocrotophos using TiO_2 and Fe^{3+}, J. Hazard. Mater. 177 (2010) 944–949, https://doi.org/10.1016/j.jhazmat.2010.01.009.

[5] M. Jagannathan, F. Grieser, M. Ashokkumar, Sonophotocatalytic degradation of paracetamol using TiO_2 and Fe^{3+}, Sep. Purif. Technol. 103 (2013) 114–118, https://doi.org/10.1016/j.seppur.2012.10.003.

[6] Y. Zhu, R. Zhu, Y. Xi, J. Zhu, G. Zhu, H. He, Strategies for enhancing the heterogeneous Fenton catalytic reactivity: a review, Appl. Catal. B Environ. 255 (2019) 117739–117754, https://doi.org/10.1016/j.apcatb.2019.05.041.

[7] Y. Zhu, R. Zhu, Y. Xi, T. Xu, L. Yan, J. Zhu, G. Zhu, H. He, Heterogeneous photo–Fenton degradation of bisphenol A over Ag/AgCl/ferrihydrite catalysts under visible light, Chem. Eng. J. 346 (2018) 567–577, https://doi.org/10.1016/j.cej.2018.04.073.

[8] Y. Zhang, M. Zhou, A critical review of the application of chelating agents to enable Fenton and Fenton–like reactions at high pH values, J. Hazard. Mater. 362 (2019) 436–450, https://doi.org/10.1016/j.jhazmat.2018.09.035.

[9] L. Chen, J. Ma, X. Li, J. Zhang, J. Fang, Y. Guan, P. Xie, Strong enhancement on Fenton oxidation by addition of hydroxylamine to accelerate the ferric and ferrous iron cycles, Environ. Sci. Technol. 45 (2011) 3925–3930, https://doi.org/10.1021/es2002748.

[10] Y. Baba, T. Yatagai, T. Harada, Y. Kawase, Hydroxyl radical generation in the photo-Fenton process: effects of carboxylic acids on iron redox cycling, Chem. Eng. J. 277 (2015) 229–241, https://doi.org/10.1016/j.cej.2015.04.103.

[11] J.S. Salla, S. Silvestri, E.M.M. Flores, E.L. Foletto, A Novel application of Cu_2FeSnS_4 particles prepared by solvothermal route as solar photo–Fenton catalyst, Mater. Lett. 228 (2018) 160–163, https://doi.org/10.1016/j.matlet.2018.06.004.

[12] Y.A. Wang, N. Bao, A. Gupta, Shape–controlled synthesis of semiconducting $CuFeS_2$ nanocrystals, Solid State Sci. 12 (2010) 387–390, https://doi.org/10.1016/j.solidstatesciences.2009.11.019.

[13] P. Ranjan, P. Kumar, T. Chakraborty, M. Sharma, S. Sharma, A study of structure and electronic properties of chalcopyrite semiconductor invoking Density Functional Theory, Mater. Chem. Phys. 241 (2020) 122346, , https://doi.org/10.1016/j.matchemphys.2019.122346.

[14] S. Tian, J. Zhang, J. Chen, L. Kong, J. Lu, F. Ding, Y. Xiong, $Fe_2(MoO_4)_3$ as an effective photo–Fenton–like catalyst for the degradation of anionic and cationic dyes in a wide pH range, Ind. Eng. Chem. Res. 52 (2013) 13333–13341, https://doi.org/10.1021/ie401522a.

[15] H. Lee, H.J. Lee, J. Seo, H.–E. Kim, Y.K. Shin, J.–H. Kim, C. Lee, Activation of oxygen and hydrogen peroxide by copper(II) coupled with hydroxylamine for oxidation of organic contaminants, Environ. Sci. Technol. 50 (2016) 8231–8238, https://doi.org/10.1021/acs.est.6b02067.

[16] C. Lee, H. Javed, D. Zhang, J. Kim, P. Westerhoff, Q. Li, P.J.J. Alvarez, Porous electrospun fibers embedding TiO_2 for adsorption and photocatalytic degradation of water pollutants, Environ. Sci. Technol. 52 (2018) 4285–4293, https://doi.org/10.1021/acs.est.7b06508.

[17] M.–Q. Yang, Y. Zhang, N. Zhang, Z.–R. Tang, Y.–J. Xu, Visible–light–driven oxidation of primary C–H bonds over CdS with dual co–catalysts graphene and TiO_2, Sci. Rep. 3 (2013) 1–7, https://doi.org/10.1038/srep03314.

[18] J. Zhang, Y. Nosaka, Quantitative detection of OH radicals for investigating the reaction mechanism of various visible–light TiO_2 photocatalysts in aqueous suspension, J. Phys. Chem. C. 117 (2013) 1383–1391, https://doi.org/10.1021/jp3105166.

[19] R.B. Castillo, J.M. Fontmorin, W. Tang, X. Dominguez–Benetton, M. Sillanpää, Towards reliable quantification of hydroxyl radicals in the Fenton reaction using chemical probes, RSC Adv. 8 (2018) 5321–5330, https://doi.org/10.1039/c7ra13209c.

[20] S. Nagarajan, N.C. Skillen, F. Fina, G. Zhang, C. Randorn, L.A. Lawton, J.T.S. Irvini, P.K.J. Robertson, Comparative assessment of visible light and UV active photocatalysts by hydroxyl radical quantification, J. Photoch. Photobio. A. 334 (2017) 13–19, https://doi.org/10.1016/j.jphotochem.2016.10.034.

[21] R.F.P. Nogueira, M.C. Oliveira, W.C. Paterlini, Simple and fast spectrophotometric determination of H_2O_2 in photo–Fenton reactions using metavanadate, Talanta 66 (2005) 86–91, https://doi.org/10.1016/j.talanta.2004.10.001.

[22] S. Guo, G. Zhang, C.Y. Jimmy, Enhanced photo–Fenton degradation of rhodamine B using graphene oxide–amorphous $FePO_4$ as effective and stable heterogeneous catalyst, J. Colloid Interface Sci. 448 (2015) 460–466, https://doi.org/10.1016/j.jcis.2015.02.005.

[23] X. Xu, D. Tang, J. Cai, B. Xi, Y. Zhang, L. Pi, X. Mao, Heterogeneous activation of peroxymonocarbonate by chalcopyrite ($CuFeS_2$) for efficient degradation of 2,4-dichlorophenol in simulated groundwater, Appl. Catal. B Environ. 251 (2019) 273–282, https://doi.org/10.1016/j.apcatb.2019.03.080.

[24] K. Chen, C. Chiang, D. Ray, Hydrothermal synthesis of chalcopyrite using an environmental friendly chelating agent, Mater. Lett. 95 (2013) 172–174, https://doi.org/10.1016/j.matlet.2012.12.100.

[25] K.M. Deen, E. Asselin, Differentiation of the non-faradaic and pseudocapacitive electrochemical response of graphite felt/$CuFeS_2$ composite electrodes, Electrochim. Acta 212 (2016) 979–991, https://doi.org/10.1016/j.electacta.2016.

07.083.
[26] A. Phaniendra, D.B. Jestadi, L. Periyasamy, Free radicals: properties, sources, targets, and their implication in various diseases, Indian J. Clin. Biochem. 30 (2014) 11–26, https://doi.org/10.1007/s12291–014–0446–0.
[27] G. Zeng, C. Zhang, G. Huang, J. Yu, Q. Wang, J. Li, B. Xi, H. Liu, Adsorption behavior of bisphenol A on sediments in Xiangjiang River, central–south China, Chemosphere 65 (2006) 1490–1499, https://doi.org/10.1016/j.chemosphere.2006.04.013.
[28] C. Davoisne, H. Leroux, M. Frère, J. Gimbolt, L. Gengembre, Z. Djouadi, V. Ferreiro, L. d'Hendecourt, A. Jones, Chemical and morphological evolution of a silicate surface under low–energy ion irradiation, Astron. Astrophys. 482 (2008) 541–548, https://doi.org/10.1051/0004–6361:20078964.
[29] H. Lv, H. Zhao, T. Cao, L. Qian, Y. Wang, G. Zhao, Efficient degradation of high concentration azo–dye wastewater by heterogeneous Fenton process with iron–based metal–organic framework, J. Mol. Catal. A Chem. 400 (2015) 81–89, https://doi.org/10.1016/j.molcata.2015.02.007.
[30] A. Ghahremaninezhad, D.G. Dixon, E. Asselin, Electrochemical and XPS analysis of chalcopyrite ($CuFeS_2$) dissolution in sulfuric acid solution, Electrochim. Acta. 87 (2013) 97–112, https://doi.org/10.1016/j.electacta.2012.07.119.
[31] X. Zhang, Y. Ding, H. Tang, X. Han, L. Zhu, N. Wang, Degradation of bisphenol A by hydrogen peroxide activated with $CuFeO_2$ microparticles as a heterogeneous Fenton–like catalyst: efficiency, stability and mechanism, Chem. Eng. J. 236 (2014) 251–262, https://doi.org/10.1016/j.cej.2013.09.051.
[32] Y. Zhang, Z. Chen, P. Wu, Y. Duan, L. Zhou, Y. Lai, F. Wang, S. Li, Three–dimensional heterogeneous electro–Fenton system with a novel catalytic particle electrode for bisphenol A removal, J. Hazard. Mater. (2019), https://doi.org/10.1016/j.jhazmat.2019.03.067 In Press.
[33] M. Sasaki, J. Maki, K. Oshiman, Y. Matsumura, T. Tsuchido, Biodegradation of bisphenol A by cells and cell lysate from *Sphingomonas* sp. Strain AO1, Biodegradation 16 (2005) 449–459, https://doi.org/10.1007/s10532–004–5023–4.
[34] P. Zhong, Q. Yu, J. Zhao, X. Shuang, X. Qiu, J. Chen, Degradation of bisphenol A by Fe–Al layered double hydroxides: a new synergy of homo and heterogeneous Fenton systems, J. Colloid Interface Sci. 552 (2019) 122–133, https://doi.org/10.1016/j.jcis.2019.05.040.
[35] V. Cleveland, J. Bingham, E. Kan, Heterogeneous Fenton degradation of bisphenol A by carbon nanotube–supported Fe_3O_4, Sep. Purif. Technol. 133 (2014) 388–395, https://doi.org/10.1016/j.seppur.2014.06.061.
[36] M. Molkenthin, T. Olmez–Hanci, M.R. Jekel, I. Arslan–Alaton, Photo–fenton–like treatment of BPA: effect of UV light source and water matrix on toxicity and transformation products, Water Res. 47 (2013) 5052–5064, https://doi.org/10.1016/j.watres.2013.05.051.
[37] U.J. Ahile, R.A. Wuana, A.U. Itodo, R. Sha'Ato, R.F. Dantas, A review on the use of chelating agents as an alternative to promote photo–fenton at neutral pH: current trends, knowledge gap and future studies, Sci. Total Environ. (2019), https://doi.org/10.1016/j.scitotenv.2019.134872 In Press.